electronics

MDPI

Review

Actively MEMS-Based Tunable Metamaterials for Advanced and Emerging Applications

Rui-Jia Xu and Yu-Sheng Lin *

School of Electronics and Information Technology, Sun Yat-sen University, Guangzhou 510006, China; xurj6@mail2.sysu.edu.cn

* Correspondence: linyoush@mail.sysu.edu.cn

Abstract: In recent years, tunable metamaterials have attracted intensive research interest due to their outstanding characteristics, which are dependent on the geometrical dimensions rather than the material composition of the nanostructure. Among tuning approaches, micro-electro-mechanical systems (MEMS) is a well-known technology that mechanically reconfigures the metamaterial unit cells. In this study, the development of MEMS-based metamaterial is reviewed and analyzed based on several types of actuators, including electrothermal, electrostatic, electromagnetic, and stretching actuation mechanisms. The moveable displacement and driving power are the key factors in evaluating the performance of actuators. Therefore, a comparison of actuating methods is offered as a basic guideline for selecting micro-actuators integrated with metamaterial. Additionally, by exploiting electro-mechanical inputs, MEMS-based metamaterials make possible the manipulation of incident electromagnetic waves, including amplitude, frequency, phase, and the polarization state, which enables many implementations of potential applications in optics. In particular, two typical applications of MEMS-based tunable metamaterials are reviewed, i.e., logic operation and sensing. These integrations of MEMS with metamaterial provide a novel route for the enhancement of conventional optical devices and exhibit great potentials in innovative applications, such as intelligent optical networks, invisibility cloaks, photonic signal processing, and so on.

Keywords: metamaterials; metasurfaces; nanophotonics; nano/microstructures; MEMS

Citation: Xu, R.-J.; Lin, Y.-S. Actively MEMS-Based Tunable Metamaterials for Advanced and Emerging Applications. *Electronics* **2022**, *11*, 243. https://doi.org/10.3390/electronics11020243

Academic Editor: Alessandro Gabrielli

Received: 2 November 2021
Accepted: 6 December 2021
Published: 13 January 2022

1. Introduction

Metamaterial, an artificial periodic micro/nanostructure used to manipulate the propagation of electromagnetic (EM) waves, has drawn a great deal of attention due to its unique electromagnetic properties [1–3]. By properly engineering the geometrical dimensions and material compositions of their subwavelength periodic unit cells, the permittivity and permeability of metamaterials can be manually controlled. Owing to that, metamaterials are widely studied in cloaking devices, energy harvesting, medical imaging, negative refraction index, and so on [4–6]. The operating wavelength range of metamaterials can be spanned in the entire EM spectrum by physically scaling the geometry, starting from visible light [7–10] to infrared (IR) [11–14], terahertz (THz) [15–20], and microwaves [21–24]. Many metamaterial-based optical devices have been demonstrated to have powerful performances [25–28]. However, these rigid devices cannot be actively tuned once fabricated. The controllable metamaterials help to improve flexibility by using an external stimulus. To satisfy this requirement, there are many techniques proposed for tuning mechanisms, including micro-electro-mechanical systems (MEMS) technology [29], thermal annealing [30], phase-transition materials [31–33], two-dimensional material [34–36], laser pumping [37], and liquid crystals [38]. Among these, MEMS technology is a promising technique for actively tunable metamaterial due to its ability to directly modify the metamaterial unit cells. Moreover, MEMS tuning methods can provide an ideal platform for metamaterial, which is not limited by the nonlinear characteristic of natural materials and exhibits a large tuning range of resonant frequency [39,40].

In recent years, active MEMS-based tunable metamaterial has become a hotspot in optoelectronics research as it provides the possibility to manually manipulate electromagnetic waves. By utilizing MEMS technologies, the metamaterial can be directly reconfigured and achieve wide applicability. Figure 1 illustrates the development of MEMS-based metamaterials in the last ten years, which indicates the diversification growth of MEMS tuning methods. In 2011, the geometric dimension of metamaterial was horizontally modified by exploiting the MEMS comb-drive actuator platform. Owing to that, Zhu et al. proposed a THz micro-ring metamaterial to achieve a large tuning range and the change of polarization-dependent states [41]. In 2012, by changing the configuration to the Maltese-cross pattern, they demonstrated a THz metamaterial with anisotropy tunable from positive to negative values [42], which showed the various applications of a stable MEMS-based metamaterial platform. In 2013, Liu et al. exhibited a mechanically actuated metamaterial capable of high-speed intensity modulation of IR radiation in a reflection configuration [43]. In the same year, Lin et al. demonstrated continuously tunable stress-induced curved cantilevers to form double split-ring resonators (DSRR) in a three-dimensional configuration to provide a higher tuning range of resonant frequency [44]. Since metamaterial can be highly integrated with MEMS technology, it is possible for metamaterial to be implanted in the actuator design. In 2015, Pitchappa et al. proposed interpixelated MEMS metamaterials for the realization of excellent switching performance [45]. Such switchable characteristics enable the realization of programmable metamaterials with higher intelligence. Along with the development of digital metamaterial, they demonstrated the microcantilevers integrated into a single unit cell for independent control of the orthogonal THz polarization response in 2016 [46]. Since then, the reconfigurable characteristic of MEMS-based metamaterial has been desired for its significant application, such as logic operation and sensing. In 2017, Liu et al. proposed a reconfigurable room temperature metamaterial IR emitter, whose displaying pixel is composed of MEMS metamaterial [47]. While the scope of application in MEMS-based metamaterial is gradually enlarged, Zhao et al. presented a tunable cantilever metasurface array to be used as a CMOS-compatible tunable quarter-wave plate in 2018 [48]. In 2019, Xu et al. demonstrated a stretchable THz parabolic-shaped metamaterial based on polydimethylsiloxane (PDMS) substrate and showed that flexible substrate can be exploited to mechanically control the metamaterial with high efficiency [49]. Mo et al. proposed a face-to-face chevron-shaped metamaterial to achieve vertical and horizontal tunings in 2020 [50]. In 2021, to enlarge the incident angle of received light and enhance the switching performance, Xu et al. proposed an actively tunable optical metadevice by integrating self-assembly electrothermal actuator and magnetic metamaterial [51]. Such a magnetic actuating method provides an ideal MEMS-based metamaterial platform with a large tilt angle and displacement. These milestone developments of actively MEMS-based metamaterial contribute a lot to the widespread applications of tunable optical devices, such as logic operation, sensing, energy harvest, display, and so on [52–57].

Since MEMS-based metamaterials in optoelectronic applications have been rapidly developed in the past decade, the actively tunable metamaterials using different MEMS tuning mechanisms are reviewed in this paper, and the outstanding characteristics of each method are summarized. The main emerging applications are discussed subsequently, i.e., logic operation and high-efficient sensing.

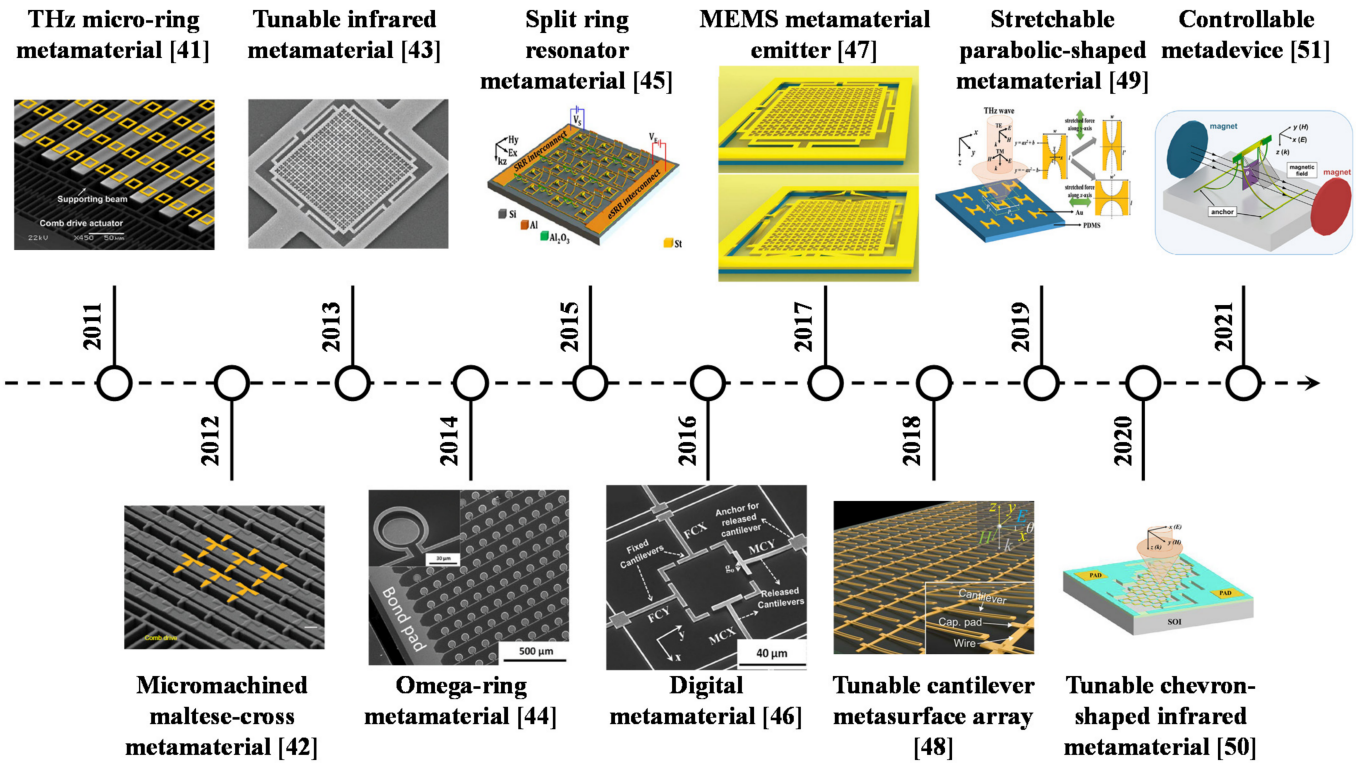

Figure 1. The development of MEMS-based tunable metamaterial in the last ten years.

2. MEMS-Based Metamaterial Emerging

The typical MEMS-based metamaterials exploit several actuating methods, including electrostatic actuators (ESAs), electrothermal actuators (ETAs), and electromagnetic actuators (EMAs). The stretchable MEMS-based metamaterials are realized by simply using a flexible substrate.

2.1. ETA-Based Metamaterial

2.1.1. Vertical Tuning Methods

The geometrical dimension is a key factor to determine the EM wave characteristics of a metamaterial. Since the first ETA-based reconfigurable THz metamaterials were demonstrated by using a thermal stimulus, as shown in Figure 2a, ETA vertical tuning methods have been widely applied in metamaterials for large physical displacement [58]. Such methods are mainly based on microcantilevers to support the continuous tuning states of lifting up and lifting down. The microcantilevers are required to comprise a multi-layer with a large difference in thermal expansion coefficients between various materials. Through the heating process, the various thermal expansions provide tensile and compressive residual stress between different layers. Thus, ETAs can be deformed upwards by an initial strain force to perform a prestressed state. Figure 2b shows the electrical split-ring resonators (eSRR) based on metamaterial microarray [59]. With the increased external temperature from 77 K to 400 K, the resonant frequency can be continuously red-shifted 80 GHz for the advanced manipulation of THz waves. Meanwhile, ETAs are widely reported to modify the vertical gap between different metamaterial layers, as shown in Figure 2c,d [60,61]. In such designs, strong coupling resonances are induced between vertical layers. Thus, the vertical displacement of ETA is exploited to control the electromagnetic properties of metamaterials.

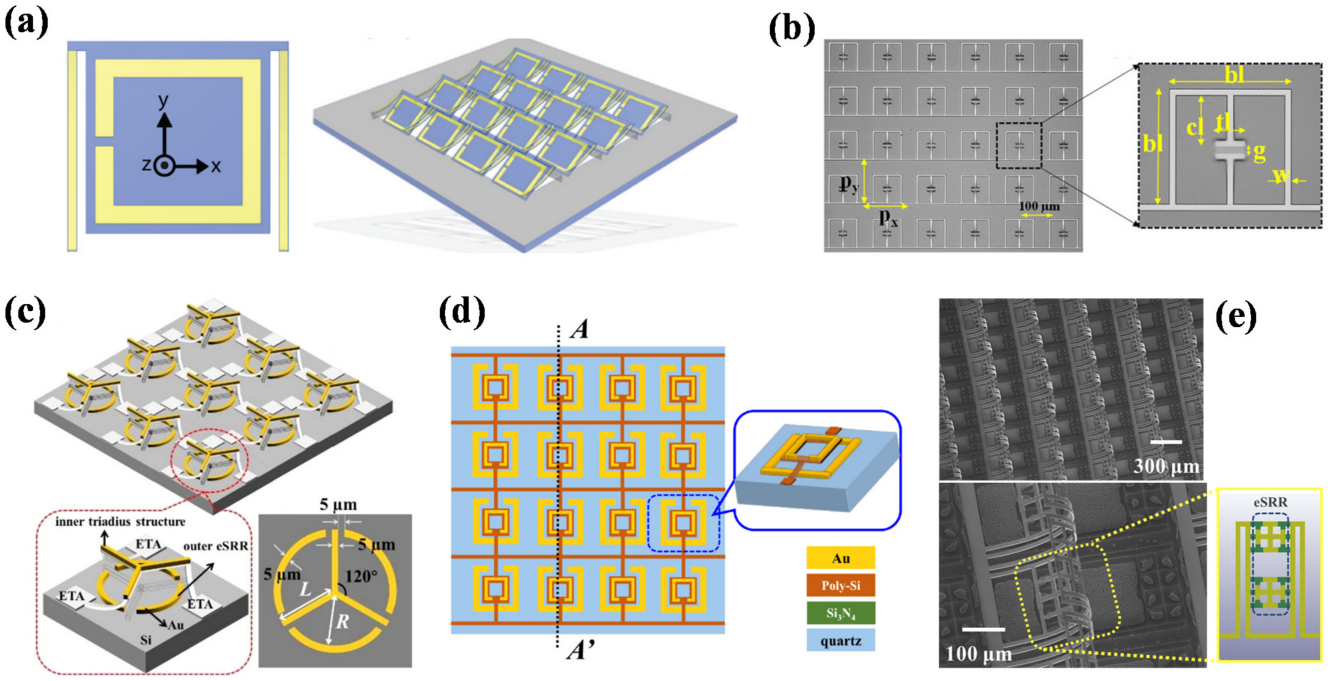

Figure 2. ETA-based vertical tuning methods of metamaterials: (**a**) schematic of thermally tunable split-ring resonators (SRR) based on the pre-stressed metamaterial [58]; (**b**) optical microscopy image of the eSRR based on metamaterial microarray [59]; (**c**,**d**) schematic of MEMS-based tunable THz metamaterial and unit cell by using ETA vertical tuning platforms [60,61]; (**e**) scanning electron microscope (SEM) images of eSRR–WCM array and unit cell [62].

While the external heating process is incompatible with CMOS-based devices, the voltage-controllable ETA tuning methods are desired to improve integration. Thus, resistance heat is exploited to increase the temperature of ETA. By applying voltage on the ETA-based metamaterial, a large amount of resistance heat can be induced by current flow to directly control the deformed height of ETA. Moreover, such voltage-controllable methods are reconfigurable. Figure 2e shows a winding-shaped cantilever metamaterial (WCM) array integrated with eSRR under a pre-deformed state [62]. The metamaterial layer is tailored to conduct the resistance heat—which can be induced—and the deformed height of ETA and then actively become tuned by applying a DC voltage. By modifying the driving voltage, the propagation of EM waves can be manually controlled to achieve electric-optical modulation. Such an ETA-based vertical tuning method provides a cost-effective platform to design metamaterials with a large tuning range.

2.1.2. Horizontal Tuning Methods

ETAs can further provide horizontal displacement for tunable metamaterial by using a chevron beam and a hot-cold arm. The chevron beam ETA is a typical design in MEMS actuators. By applying a voltage on the ends of ETAs to increase the temperature, the center shuttle of actuators can be moved due to the thermal expansion on both sides of the chevron beams. Figure 3a indicates a tunable metamaterial based on a two-cut SRR unit cell and the tuning mechanism [63]. While the center shuttle of the chevron beam actuator generates a displacement, the slabs move towards the cuts of the two-cut SRR, which achieves a continuous tuning method for the metamaterial by changing the gap between slabs and SRR. A reconfigurable THz metamaterial is obtained from the embedment of a chevron beam ETA as shown in Figure 3b [64]. By applying the appropriate actuation voltage on ETAs, the enhanced bandwidth tunability at two different resonances can be accomplished.

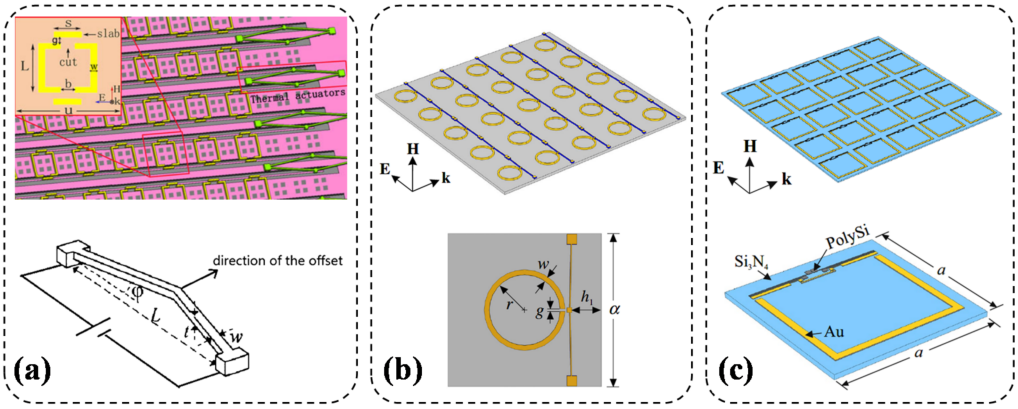

Figure 3. ETA-based horizontal tuning methods of metamaterial: (**a**) schematic of the tunable metamaterials and the two-cut SRR unit cell [63]; (**b**) schematic of tunable metamaterial and the unit cell using the chevron beam ETA [64]; (**c**) schematic of two independent ETA, SRR, and unit cell [65].

The cold-hot-arm based ETAs can achieve the increment of power consumption efficiency and larger curvature compared with the design of chevron beam ETA. In this method, by applying an external voltage, the electric current flows along the hot arms to generate resistive heating and thermal expansion. While the cold arms are not connected to the electric flowing loop and remain at low temperature, a large deflection can be induced owing to the thermal expansion difference between hot and cold arms. Figure 3c shows a tunable metamaterial based on the combination of two-hot-arm ETAs with an SRR [65]. The tuning methods provide the mu-negative behavior via a low voltage. These results prove that the horizontal ETA is a promising method for tunable metamaterial to be used in low voltage applications.

2.2. ESA-Based Metamaterial

2.2.1. Vertical Tuning Methods

ESA is a commercial and mature MEMS actuating method, which induces an electrostatic motion by driving an electrical input. To enable the vertical displacement, the electrical potential difference is usually induced between different conductive layers, i.e., a metallic layer and a semiconductor substrate. Figure 4a shows a tunable THz filter based on a DSRR structure released from a silicon substrate [66]. By applying different DC bias voltages between metallic SRR layers and silicon substrates, the bending degree of micro-cantilever can be continuously changed to realize a large frequency tuning range and high quality (Q)-factor. Meanwhile, the released SRR cantilevers will be snapped down to silicon substrate with the DC bias higher than the pull-in voltage. Liu et al. designed and experimentally demonstrated ultrathin tunable THz absorbers based on MEMS-based metamaterial, as shown in Figure 4b [67]. These were composed of a metallic ground plane, a silicon nitride spacer, and a matrix of meta-atoms from bottom to top. The metamaterial membranes were suspended above the silicon nitride layer by a distance, which was adjustable with different driving electrostatic forces. By applying a voltage, the absolute absorption modulation range measured at the initial resonance could reach 65%. In Figure 4c, a MEMS-based metasurface is demonstrated for active control of the Fano-resonances [68]. Two SRRs can be independently and sequentially actuated by applying the voltages. With multiple inputs and outputs to represent on and off digital states, such designs are suitable for logic operations at the THz frequencies. Several planar arrays of eSRR with movable stress curved beams are proposed as shown in Figure 4d,e, which are actuated out-of-plane by electrostatic force [69,70]. Figure 4f shows a tunable THz filter and a modulator based on ESA-metamaterial [71]. A radio frequency-MEMS (RF-MEMS) capacitor is embedded in the center of each SRR unit cell to tune the electromagnetic resonant frequency, while the modulation speed can reach 2 kHz. Figure 4g indicates an active MEMS metamaterial

for the THz bandwidth control, which consists of an array of sixteen cantilever resonators with gradually varying release lengths [72]. By electrostatically controlling the out-of-plane height of the released micro-cantilever-based resonators, the full width half maximum (FWHM) resonance bandwidth of the MEMS metamaterial can be actively switched to 90 GHz. With a supercell composed of several cantilevers, the switching range can be further improved, as shown in Figure 4h [73]. Each metamaterial unit cell consists of eight cantilevers placed at the corner of an octagon ring to achieve a large tuning range of 0.37 THz. Figure 4i shows a structurally reconfigurable metamaterial for active switching of near-field coupling in conductively coupled, orthogonally twisted SRRs [74]. SRRs structures are precisely tailored to excite the classical analogue of electromagnetically induced transparency (EIT) by the strong conductive coupling. In Figure 4j,k, the ESA-based tunable THz metamaterials using three-dimensional eSRR arrays are proposed to realize polarization-sensitivity and flow tuning capability, respectively [75,76]. It can be clearly observed that the ESA-based vertical tuning method provides a mature platform for metamaterial and opens an avenue for more potential applications, such as logic operation, EM wave modulation, flowing sensing, and so on [77–79].

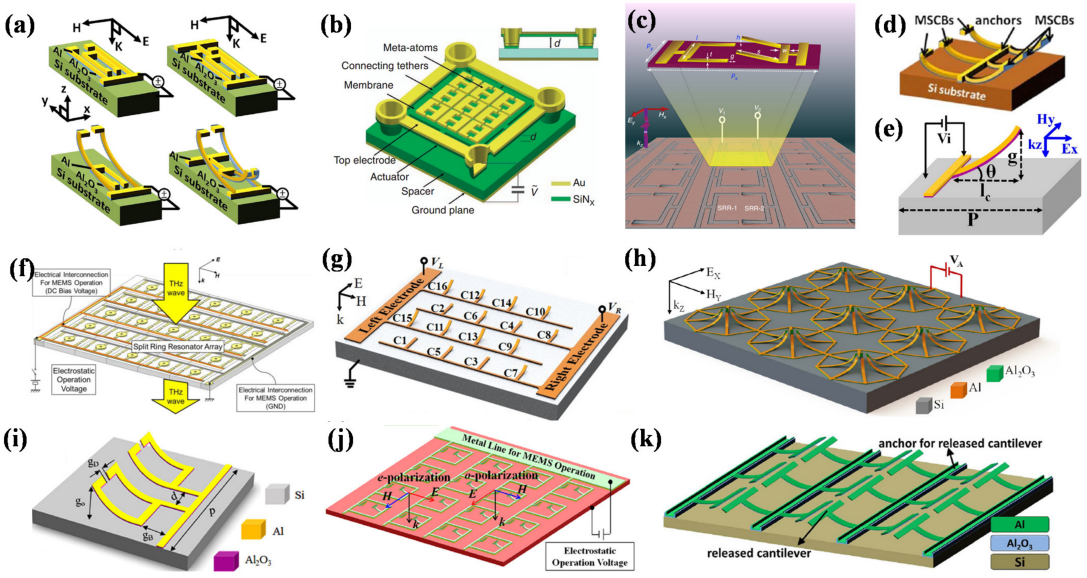

Figure 4. ESA-based vertical tuning methods of metamaterial: (**a**) schematic of DSRR with single-side and double-side ESA structure under unreleased and released state, respectively [66]; (**b**) schematic of the unit cell of the THz absorber [67]—the vertical distance between the meta-atoms and the ground plane can be tuned electrostatically; (**c**) colored SEM image of the MEMS Fano metasurface [68]—the periodic unit cell comprises of two SRRs; (**d**) schematic of electric split-ring resonators with movable stress-curved beams (eSRR-MSCBs) after microstructures are released [69]; (**e**) schematic of an upward bent microcantilever as metamaterial unit cell [70]; (**f**) MEMS reconfigurable SRR design array of the unit cell [71]; (**g**) schematics of a bandwidth tunable MEMS metamaterial supercell formed by a 4 × 4 array of microcantilever resonators with varying fixed and released lengths [72]; (**h**) schematics of the proposed uniaxially isotropic MEMS metamaterial with eight released cantilevers in an octagon ring [73]; (**i**) schematics of the conductively coupled MEMS metamaterial [74]; (**j**) schematics of the chained eSRR array with a metal line connecting the eSRRs for MEMS operation [75]; (**k**) schematic of the mirrorlike T-shape metamaterial (MTM) device after release [76].

2.2.2. Horizontal Tuning Methods

Comb driver is a typical design of ESA that is suitable to horizontally modify the geometry of metamaterial. Comb drivers are composed of fixed combs and movable combs. By applying a voltage potential difference on combs, an electrostatic force can be generated to drive a movable comb to approach a fixed comb. Moreover, the comb driver can suitably

provide a tunable platform for the whole metamaterial array to achieve better uniformity of deformation in each unit cell. Figure 5a shows reconfigurable asymmetric split-ring resonators (ASRRs) metamaterial [80]. Two identical electrostatic comb-drive actuators are employed on both sides for a mechanically balanced translation of the supporting frame, which can realize a horizontal displacement of 20 µm. Similarly, switchable ESA-based metamaterials are demonstrated by using fixed SRR and moveable SRR as shown in Figure 5b,c [81,82]. By reshaping the micromachined metamaterial unit cells, the surface resonance of the metamaterial is manually controlled. Figure 5d indicates a tunable metamaterial consisting of two SRR array layers [83]. The top SRR layer is on a movable silicon frame that can be actuated by a comb-drive actuator while the bottom SRR layer is fixed on a SiNx thin-film. By applying voltage on the comb driver, a continuous lateral shifting between the coupled resonators can be induced to 20 µm. A MEMS integrated device is proposed by using EIT metamaterial, as shown in Figure 5e [84]. The comb driver design is composed of a fixed beam and a movable beam based on a silicon on insulator (SOI) wafer. In Figure 5f, a reconfigurable metasurface is proposed to achieve both the polarization conversion and the polarization rotation in the THz frequency range by using the comb driver [85]. In the IR wavelength range, ESA-based metamaterials are also reported to realize active modulation of the polarization state, as shown in Figure 5g [86]. In Figure 5h–j, Xu et al. propose several SRR patterns integrated with the comb driver platform to be operated at different frequencies, which can be applied in many fields, such as tunable filters, frequency-selective detectors, polarization switches, high-efficient environmental sensors, and more [87–89]. From these literature reports, the ESA-based platform shows great applicability for the horizontal tunable metamaterial. The comb driver provides more mature tuning methods compared with other MEMS tuning mechanisms. The geometry of integrated metamaterial is rapidly reduced, which means the MEMS-based metamaterial can be gradually operated from THz and IR, as well as visible spectra [90].

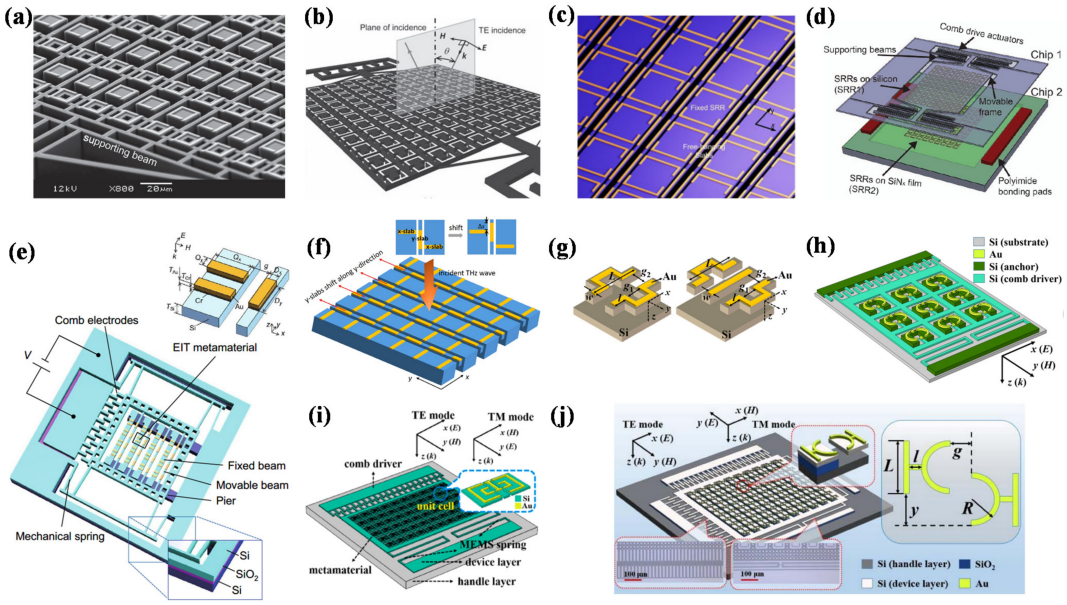

Figure 5. ESA-based horizontal tuning methods of metamaterial: (**a**) SEM images of the reconfigurable ASRRs metamaterial [80]; (**b**) schematic of the switchable magnetic metamaterial consisting of two semi-square split rings separated by a gap [81]; (**c**) schematics of the micromachined metamaterial with the element consisting of a two-cut SRR and two free-hanging slabs [82]; (**d**) schematic of the tunable metamaterials, including broadside-coupled SRRs (BC-SRRs) [83]; (**e**) schematic of the MEMS integrated device—unit cell of the EIT metamaterial consists of a cut wire and a wire pair [84]; (**f**) schematics of the tunable metasurface for the polarization conversion and the polarization rotation [85]; (**g**) schematics of polarization-sensitive IR metamaterials (PSIMs) [86]; (**h**–**j**) schematic of a tuning eSRR array by using comb drive horizontal tuning platforms [87–89].

2.3. EMA-Based Metamaterial

A change in the external magnetic field can cause a motion in EMA, which is composed of magnetic materials. Figure 6a shows a Ferrite-based magnetically tunable left-handed metamaterial by introducing yttrium iron garnet rods into SRRs/wires periodic array [91]. Thus, by using external DC applied magnetic fields, the left-handed passband of the metamaterial can be continuously and reversibly adjusted. Figure 6b indicates a low-voltage three-axis EMA-based micro-mirror to support optical devices [92]. The frame is connected to the robust torsion bar and lifting bar structure formed by bulk silicon to perform greater operating stability. A flexible and controllable metadevice is proposed by using self-assembly MEMS-based ESA, as shown in Figure 6c [51]. While the center metamaterial plate is released by the supporting arm, it can be actuated and rotated by a magnetic force to manipulate the incident electromagnetic response by driving the external electromagnetic field. Figure 6d shows a tunable THz metamaterial employing magnetically actuated cantilevers [93]. By coating a magnetic material on the cantilever surface, the released eSRR array can be actuated and the resonant frequency of the structures can be modified. These results indicate that the large displacement and rotation angle of EMA tuning methods provide a great possibility for metamaterial to receive light from a wide incident angle, which can greatly improve the sensitivity of metamaterial.

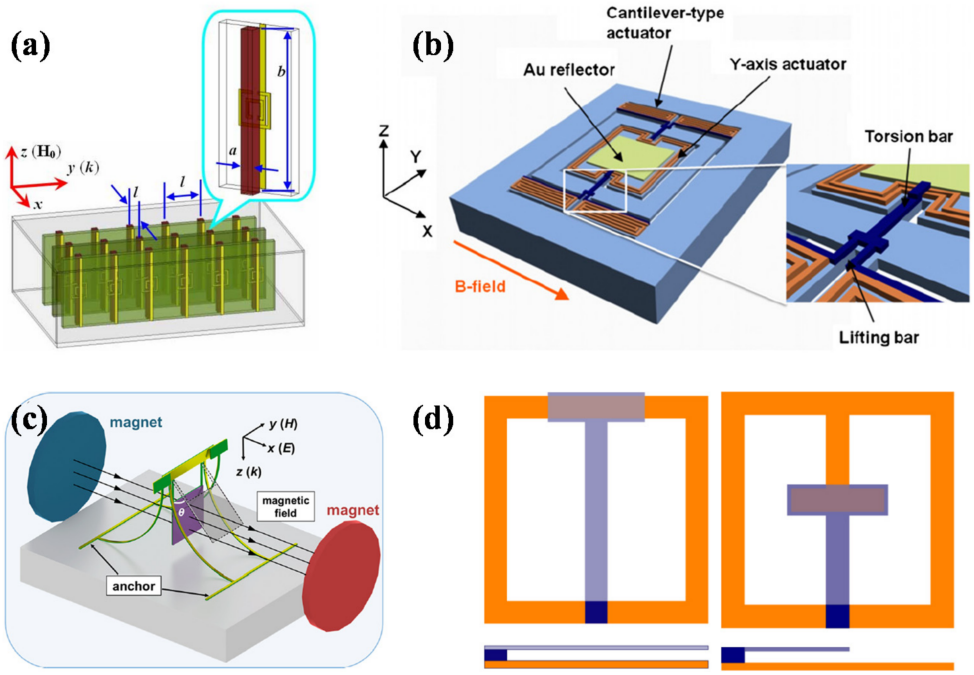

Figure 6. EMA-based tuning methods of metamaterial: (**a**) schematic of the magnetically tunable left-handed metamaterial (LHM) composed of SRRs/wires array and introducing yttrium iron garnet (YIG) rods in rectangular waveguide [91]; (**b**) schematic of the three-axis EMA-based micromirror for fine alignment among optical devices [92]; (**c**) schematic of active out-of-plane metadevice by driving a magnetic field [51]; (**d**) schematics of an eSRR modified to incorporate a parallel plate capacitor with a flexing cantilever [93].

2.4. Flexible Substrate-Based Metamaterial

In addition to the conventional MEMS actuating mechanisms, the tuning optical characteristic of metamaterial can be realized by using stretchable and flexible substrates, such as PDMS, polyimide, and polyethylene terephthalate (PET) [94–96]. It is a simpler mechanical method to provide a large tuning range of resonant frequency. Figure 7a shows a THz metamaterial comprising a planar array of I-shaped resonators on a highly elastic PDMS substrate [97]. While such resonators are sensitive to mechanical stretching,

the stretching range of metamaterial is over 8% to keep good repeatability over several stretching–relaxing cycles. Zhang et al. demonstrated a mechanically stretchable and tunable metamaterial absorber composed of a dielectric resonator stacked on a conductive rubber, illustrated in Figure 7b [98]. By applying different stretching strains to change the elementary cells' periodicity, the operation frequency of the metamaterial absorber is blue-shifted in the microwave spectrum range. A three-layered stretchable metamaterial absorber by using liquid metal and PDMS is proposed in Figure 7c [99]. The resonant frequency of the device can be increased from 18.50 GHz to 18.65 GHz, with a stretching length of 1.2 cm, which is suitable to be used as a wireless strain sensor. Figure 7d shows a plasmonic antenna-based metasurface on the stretched PDMS [100]. By precisely positioning the Au nanorods, the optical phase is varied over the individual component by a certain amount. Furthermore, the position-dependent phase discontinuity can be further tuned by stretching the metamaterial geometry for reconfigurable flat optics application. Figure 7e indicates a stretchable THz parabolic-shaped metamaterial (PSM) to perform logic operations [49]. By stretching the PSM width and length, single-/dual-band switching and polarization switching characteristics can be realized for programmable metamaterials. A tunable perfect absorber with a ring-shaped (PA-RS) and a cross-shaped (PA-CS) on PDMS substrate is proposed in Figure 7f [101]. Stretching devices into different directions allows them to exhibit ultra-narrowband, polarization-dependent/independent, and switchable characterizations in the IR wavelength range. The typical advantages of such flexible substrate-based metamaterials are their flexibility and cost-effectiveness, which makes them potentially useful in wearable devices and a variety of sensor fields [102,103].

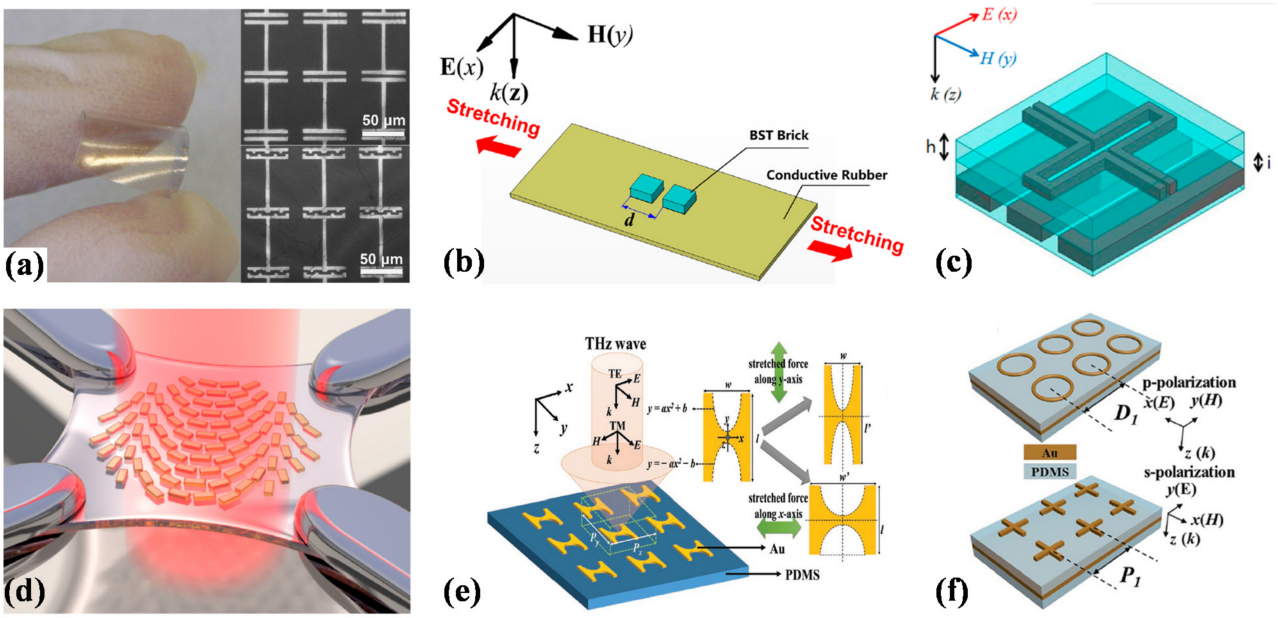

Figure 7. Flexible substrate-based metamaterial: (**a**) photograph and optical micrograph of I-shaped flexible metamaterial design [97]; (**b**) schematic of stretchable dielectric metamaterial absorber [98]; (**c**) schematics of stretchable metamaterial absorber by using liquid metal as the conductor and PDMS as the substrate [99]; (**d**) schematic of a gold nano-rod metasurface array on stretched PDMS [100]; (**e**) schematic of the PSM device operated by applying a stretching force along the x- and *y*-axis directions [49]; (**f**) schematics of stretchable perfect absorber with ring-shaped (PA-RS) and cross-shaped (PA-CS) structures [101].

2.5. Summary

The outstanding characteristics of different actuating methods are summarized in Table 1. The advantages of low driving voltage and large displacement can be realized by ETA or EMA tuning mechanisms. However, the challenge for the development of ETA

is the slow processing response. The need for external magnets and the electromagnetic interference effect are problems within EMA that cannot be easily neglected. For ESA, although the ESA-based metamaterial tuning platform is quite mature, the pull-in effect and high driving voltage greatly limit their applications. Moreover, the flexible substrate-based metamaterial is stretchable and bendable for wearable electronic applications but the fabrication is incompatible with the conventional CMOS manufacturing process. While each actuating method exhibits obvious advantages and disadvantages, they can be chosen in different fields due to the specific requirement of the application.

Table 1. Comparison of MEMS-based tuning mechanism.

Actuation Type	Advantages	Disadvantages
ETA	Low driving voltage Large displacement	Slow response
ESA	Fast response Mature fabrication	Pull-in effect High driving voltage
EMA	Low driving voltage Large displacement	Need external magnets Electromagnetic interference
Stretching mechanism	Simple fabrication Large displacement Flexible, bendable	Need flexible substrate Incompatible to CMOS process

For MEMS-based tunable metamaterials, a large tunable range and Q-factor are desired for the real application of devices. Herein, the key parameters of different demonstrated metamaterials are compared in Table 2, including their operating waveband, metamaterial pattern, tunable range, and Q-factor. It can be observed that MEMS-based metamaterial can achieve a high Q-factor of 118 when properly designed. Meanwhile, an ideal MEMS tuning platform integrated with a suitable metamaterial pattern can achieve a large tunable range to meet the various requirements of the operating wavelength. Such methods are promising to fabricate electrical devices with powerful performance. Moreover, while the MEMS-based metamaterials are mainly reported to operate at the IR/THz spectra ranges, there is rare literature demonstrating the visible light metamaterials due to their difficult manufacturing process. This means that, at the nanoscale, MEMS metamaterial possesses great potential to be applied in unexplored fields, such as micro holographic projection, visual sensing, and more.

Table 2. Comparison of MEMS-based tunable metamaterials.

Operating Waveband	Metamaterial Pattern	Tunable Range	Q-Factor	Reference
IR	Moon-shaped	1.62 μm	11	[51]
	Cross-shaped	2.37 μm	118	[101]
THz	eSRR	0.08 THz	3.2	[59]
	Parabolic-Shaped	0.55 THz	50	[49]
	eSRR	0.09 THz	66	[60]
	SRR	0.11 THz	19	[68]
	SRR	0.50 THz	10	[81]

In summary, MEMS-based metamaterials, via various actuation types, have been proved to possess powerful performance and fruitful applications. For specific requirements, MEMS-based metamaterials can be tailored to use different actuation mechanisms. Such a method of designing has gradually become more advanced, with a promise of being widely used in commercial industries. However, poor compatibility of conventional MEMS manufacturing processes to electromagnetic metamaterial is limiting the develop-

ment of MEMS-based metamaterial because of the conventional MEMS actuating platform exhibiting extremely large volumes of the electromagnetic metamaterial. The development of the fabrication process will become one of the promotion directions of MEMS-based metamaterial. Moreover, the high-power loss of metamaterial is another tough challenge that limits the maturation of MEMS-based metamaterial technology. In the future, to solve these problems, innovative materials, configurations, and tuning mechanisms need to be adopted to enhance performance and stability. Such advanced MEMS-based metamaterial devices will likely be used in various applications, such as electro-optic modulators, optical computers, and more.

3. Application

As MEMS tuning methods contribute a lot to the development of metamaterials, the active control of EM waves is gradually realized, and many potential applications are further explored. Herein, logic operation and sensing are two typical application fields of MEMS-based metamaterials.

3.1. Logic Operation

Owing to the reconfigurable and switchable characteristics of MEMS-based metamaterials, they are suitable to be used for logic operation. For example, the strong resonance intensity of the metadevice could be referred to as being in an "on" state, while the weak resonance intensity of the metadevice could be referred to be in the "off" state. Such switchable states possess the ability to represent binary signals and perform different logic operating functions [104]. In Figure 8a, Cong et al. demonstrated a MEMS-based metal–insulator–metal metamaterial cavity array, which can be actively switched between different phases by using a bimorph cantilever [105]. Figure 8b indicates a THz MEMS-based metamaterial for the active control of resonant cloaking [106]. In the "off" state of the closed ring resonator (CRR) cantilevers without a driving voltage, the transmission spectrum exhibits a strong coupling behavior at 1.1 THz. In the "on" state of the CRR cantilevers with a driving voltage of 30 volts, the transparency peak will completely disappear, while a strong dipole type of a new resonance may be induced. A reconfigurable THz wrench-shaped metamaterial (WSM) is proposed to perform the programmable characteristic as shown in Figure 8c [107]. While such metamaterials show the polarization-dependent characteristics, the binary digital signals "0" and "1" can be represented by configuring the WSM meta-atoms with different heights between the meta-atoms and substrate. Figure 8d shows a programmable multi-digital metamaterial by using SRR structure [108]. By moving the central metal bar under different polarization states, the eSRR can be logically switched. Figure 8e shows a binary coded digital metamaterial for the control of output intensities demonstrated by Ho et al. [109]. By applying a different combination of input voltages, the output at 0.26 THz shows the analogous characteristic of an NOR logical gate, while the output at 0.36 THz shows the analogous characteristic of an AND logical gate. These results enable the enhancement in the manipulation of the THz wave and the realization of programmable metamaterial for various logic operation functions.

3.2. Sensing

By exploiting the mechanical and optical characteristics, MEMS-based metamaterials have been widely used in gas sensing, photo-detecting, flow monitoring, etc. [110–120]. Such sensors can be designed to be sensitive to specific ranges of wavelengths for the requirement of different applications. Figure 9a shows the integration of the thermoelectric type MEMS IR sensor with a plasmonic metamaterial absorber (PMA) [110]. While the PMA with MIM structure exhibits the capability of absorptivity enhancement and absorption range extension, the responsivity of the MEMS thermoelectric IR sensor can be further increased by 20%. Figure 9b indicates an ultrathin plasmonic metasurface for spectrally selective IR sensing applications [111]. By simultaneously tailoring optical and electromechanical properties, a high thermomechanical coupling can be realized to selectively detect

the long-wavelength IR radiation. A split-disk metamaterials (SDMs) array is proposed in Figure 9c [112]. By changing the environmental refraction index, SDM exhibits a high sensitivity of 3312 nm/RIU and is suitable to be used as a high-efficient and high-sensitive gas sensor and biosensor. Figure 9d shows a multi-band flexible metamaterial based on PDMS substrate to perform curvature sensing functionality [113]. The relationship of the frequency shift and amplitude modulation is provided as a function of the applied bending strain to realize a strain sensor. Figure 9e indicates a tunable PMA consisting of an eSRR and a cross-shaped nanostructure based on dipole and inductive–capacitive (LC) resonances [114]. The absorption resonance can be red-shifted by increasing the value of the refraction index, and the sensitivity to the refraction index reaches 1200 nm/RIU. Lin et al. demonstrated mirrorlike T-shaped metamaterial (MTM) with out-of-plane movable microstructures to perform flow sensing application [76], displayed in Figure 9f. By applying the fluidic flowing pressure, the released MTM cantilevers can be deflected at different bending states and induce the variation range of the resonant frequency to detect the flow rate. The sensing performance of metamaterial can be greatly improved to enlarge the applying fields by using MEMS techniques, such as refractive index sensing, flowing rate sensing, thermo-sensing, photo-sensing, and so on [115–120].

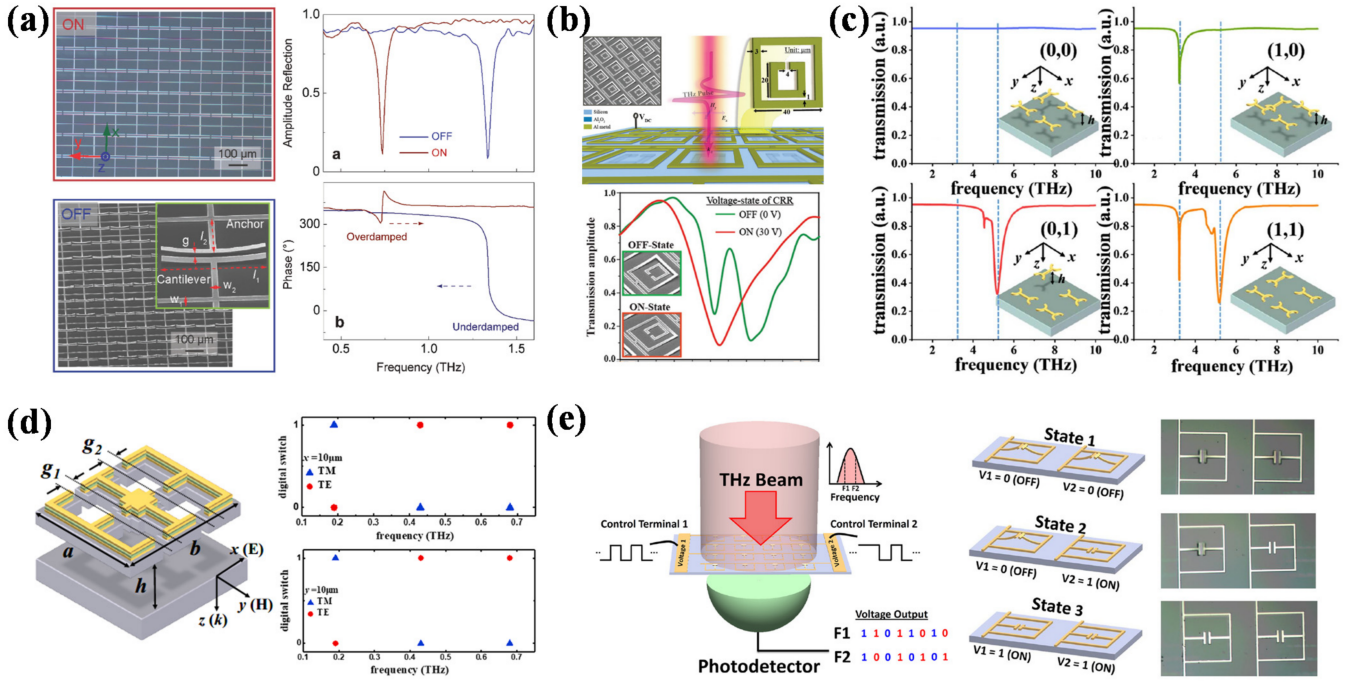

Figure 8. MEMS-based metamaterial for logic operation. (**a**) The "on" and "off" states microscopic images of the MEMS-based metamaterial array [105]. The reflection amplitude spectra and the phase spectra of the MEMS-based MIM metamaterial operating in the "on" and "off" states. (**b**) Schematic of the MEMS-incorporated composite reconfigurable metamaterial structure consisting of outer MEMS CRR and the inner SRR [106]. THz transmission spectra of the composite MEMS-metamaterial device without and with the driving voltage across the metal lines and the silicon substrate. (**c**) Programmable metamaterial using the WSM configuration for (0, 0), (1, 0), (0, 1), and (1, 1), respectively [107]. (**d**) Schematic of eSRR, which can logically switch the digital signals as (0, 1) and (1, 0) at different polarization states and switch the digital signals as (0, 0) and (1, 1) by moving the central bar along the x- and *y*-axis, respectively [108]. (**e**) Schematic of the proposed binary coded digital metamaterial for the control of output intensities at specific frequencies to provide the analogous logic outputs [109].

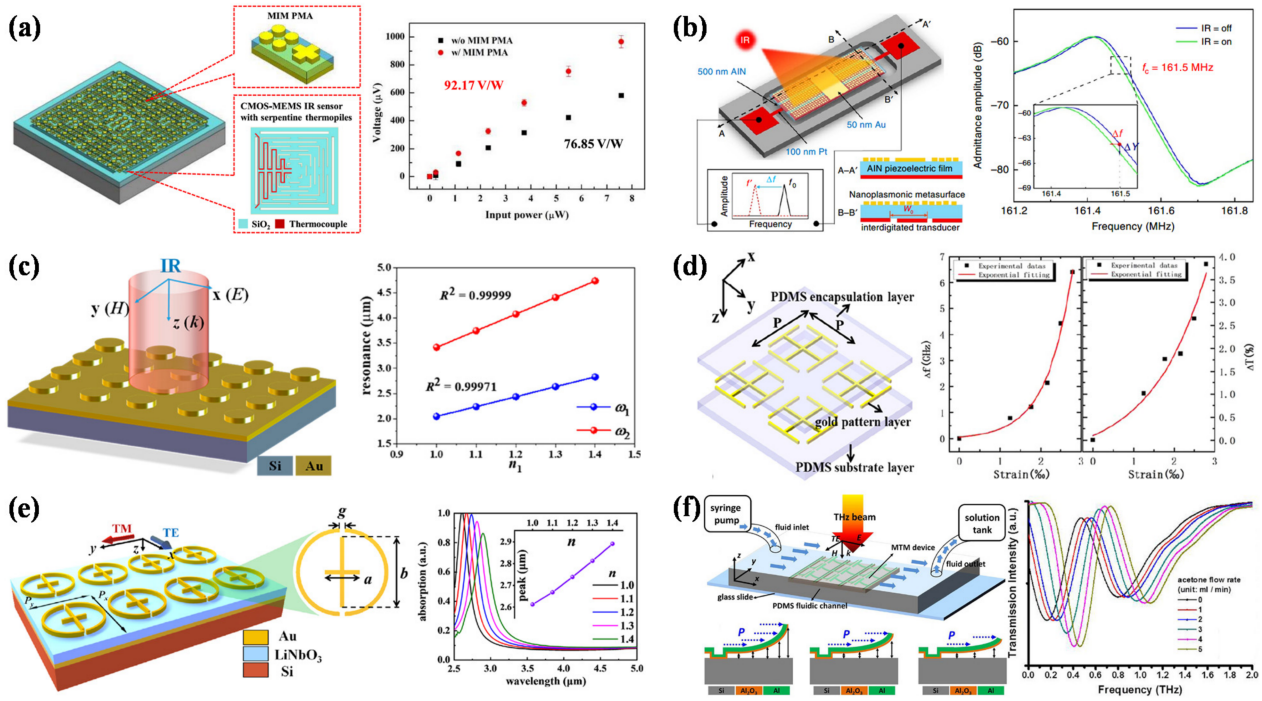

Figure 9. MEMS-based metamaterial for sensing applications. (**a**) Schematic of MEMS IR sensor integrated with MIM-based PMA [110]. The responsivity of IR sensors is determined from the measured output voltage and input power. (**b**) Schematic of plasmonic piezoelectric nanomechanical resonant IR detector [111]. Measured admittance curves versus frequency of the resonator for IR on and off states. (**c**) Schematic of SDM and the application for refraction index sensing [112]. (**d**) Schematic of the metamaterial strain sensor with a sandwich structure [113]. The relationship between frequency shift (Δf), amplitude modulation (ΔT) and strain. (**e**) Schematic of tunable PMA and the application for refraction index sensing [114]. (**f**) Schematic of the MTM device integrated with a PDMS fluidic channel [76]. The initial, intermediate, and final state of an MTM cantilever with respect to low, medium, and high flow rates, respectively. The flow tuning characteristic of the MTM device under acetone solutions.

4. Conclusions

With the rapid development of metamaterial in optoelectronic devices, MEMS-based metamaterials are widely studied to achieve the active control of EM waves and satisfy the requirements of real-world applications. For these devices, actuating method is a key factor to determine the performance, such as tuning range, driving power, operating frequency, fabrication compatibility, and more. The actuation methods can mainly be divided into ETA, ESA, EMA, and stretching mechanisms. While each actuation method exhibits obvious advantages and disadvantages, the choices of tuning methods are required to be well-considered in metamaterial for different applications. MEMS-based metamaterials have brought up the possibility for the manipulation of incident EM waves, including amplitude, frequency, phase, and polarization state. Meanwhile, the operating frequency range is further spanned from visible to IR and THz spectra ranges, which enables many efficient implementations of optical devices, e.g., logic operation and sensing devices. Although the advanced application of MEMS-based metamaterial is fruitful, the high-power loss and poor compatibility in the current IC manufacturing process are still tough challenges that limit the maturation of MEMS-based metamaterial technology in the commercial industry. The future looks promising in the development of MEMS-based metamaterials that overcome these limitations by implanting innovative materials, configurations, and tuning mechanisms. Therefore, MEMS-based metamaterial technology can be integrated

into the current optoelectronic devices to achieve a large enhancement of performance, such as electro-optic modulators, optical computers, on-chip detectors, and more.

Author Contributions: Conceptualization, R.-J.X.; data curation, R.-J.X.; writing—original draft preparation, R.-J.X.; writing—review and editing, R.-J.X. and Y.-S.L.; supervision, R.-J.X. and Y.-S.L.; project administration, Y.-S.L.; funding acquisition, Y.-S.L. All authors have read and agreed to the published version of the manuscript.

Funding: This research was funded by the Natural Science Foundation of Basic and Applied Foundation of Guangdong Province, grant number 2021A1515012217; the National Key Research and Development Program of China, grant number 2019YFA0705004; the National Natural Science Foundation of China, grant number 11690031.

Acknowledgments: The authors acknowledge the State Key Laboratory of Optoelectronic Materials and Technologies of Sun Yat-Sen University for the use of experimental equipment.

Conflicts of Interest: The authors declare no conflict of interest.

References

1. Smith, D.R.; Pendry, J.B.; Wiltshire, M.C.K. Metamaterials and negative refractive index. *Science* **2004**, *305*, 788–792. [CrossRef] [PubMed]
2. Chen, H.T.; Padilla, W.J.; Zide, J.M.; Gossard, A.C.; Taylor, A.J.; Averitt, R.D. Active terahertz metamaterial devices. *Nature* **2006**, *444*, 597–600. [CrossRef] [PubMed]
3. Schurig, D.; Mock, J.J.; Justice, B.J.; Cummer, S.A.; Pendry, J.B.; Starr, A.F.; Smith, D.R. Metamaterial electromagnetic cloak at microwave frequencies. *Science* **2006**, *314*, 977–980. [CrossRef]
4. Cui, Y.; Fung, K.H.; Xu, J.; Ma, H.; Jin, Y.; He, S.; Fang, N.X. Ultrabroadband light absorption by a sawtooth anisotropic metamaterial slab. *Nano Lett.* **2012**, *12*, 1443–1447. [CrossRef] [PubMed]
5. Fu, K.; Zhao, Z.; Jin, L. Programmable granular metamaterials for reusable energy absorption. *Adv. Funct. Mater.* **2019**, *29*, 1901258. [CrossRef]
6. Le, D.H.; Lim, S. Four-mode programmable metamaterial using ternary foldable origami. *ACS Appl. Mater. Interfaces* **2019**, *11*, 28554–28561. [CrossRef]
7. Li, W.; Guler, U.; Kinsey, N.; Naik, G.V.; Boltasseva, A.; Guan, J.; Shalaev, V.M.; Kildishev, A.V. Refractory plasmonics with titanium nitride: Broadband metamaterial absorber. *Adv. Mater.* **2014**, *26*, 7959–7965. [CrossRef]
8. Ma, H.; Song, K.; Zhou, L.; Zhao, X. A naked eye refractive index sensor with a visible multiple peak metamaterial absorber. *Sensors* **2015**, *15*, 7454–7461. [CrossRef]
9. Ni, X.J.; Wong, Z.J.; Mrejen, M.; Wang, Y.; Zhang, X. An ultrathin invisibility skin cloak for visible light. *Science* **2015**, *349*, 1310–1314. [CrossRef]
10. Esposito, M.; Tasco, V.; Todisco, F.; Cuscuna, M.; Benedetti, A.; Scuderi, M.; Nicotra, G.; Passaseo, A. Programmable extreme chirality in the visible by helix-shaped metamaterial platform. *Nano Lett.* **2016**, *16*, 5823–5828. [CrossRef]
11. Hossain, M.M.; Jia, B.; Gu, M. A metamaterial emitter for highly efficient radiative cooling. *Adv. Opt. Mater.* **2015**, *3*, 1047–1051. [CrossRef]
12. Su, Z.; Yin, J.; Zhao, X. Soft and broadband infrared metamaterial absorber based on gold nanorod/liquid crystal hybrid with tunable total absorption. *Sci. Rep.* **2015**, *5*, 16698. [CrossRef] [PubMed]
13. Dao, T.D.; Ishii, S.; Yokoyama, T.; Sawada, T.; Sugavaneshwar, R.P.; Chen, K.; Wada, Y.; Nabatame, T.; Nagao, T. Hole array perfect absorbers for spectrally selective midwavelength infrared pyroelectric detectors. *ACS Photonics* **2016**, *3*, 1271–1278. [CrossRef]
14. Kim, J.; Han, K.; Hahn, J.W. Selective dual-band metamaterial perfect absorber for infrared stealth technology. *Sci. Rep.* **2017**, *7*, 6740. [CrossRef] [PubMed]
15. Cong, L.; Xu, N.; Gu, J.; Singh, R.; Han, J.; Zhang, W. Highly flexible broadband terahertz metamaterial quarter-wave plate. *Laser Photonics Rev.* **2014**, *8*, 626–632. [CrossRef]
16. Yang, K.; Liu, S.; Arezoomandan, S.; Nahata, A.; Sensale-Rodriguez, B. Graphene-based tunable metamaterial terahertz filters. *Appl. Phys. Lett.* **2014**, *105*, 093105. [CrossRef]
17. Yao, G.; Ling, F.; Yue, J.; Luo, C.; Ji, J.; Yao, J. Dual-band tunable perfect metamaterial absorber in the THz range. *Opt. Express* **2016**, *24*, 1518–1527. [CrossRef]
18. Wang, B.-X.; Wang, G.-Z. Temperature tunable metamaterial absorber at THz frequencies. *J. Mater. Sci. Mater. Electron.* **2017**, *28*, 8487–8493. [CrossRef]
19. Huang, M.; Cheng, Y.; Cheng, Z.; Chen, H.; Mao, X.; Gong, R. Based on graphene tunable dual-band terahertz metamaterial absorber with wide-angle. *Opt. Commun.* **2018**, *415*, 194–201. [CrossRef]
20. Liu, G.D.; Zhai, X.; Meng, H.Y.; Lin, Q.; Huang, Y.; Zhao, C.J.; Wang, L.L. Dirac semimetals based tunable narrowband absorber at terahertz frequencies. *Opt. Express* **2018**, *26*, 11471–11480. [CrossRef] [PubMed]

21. Ding, F.; Cui, Y.; Ge, X.; Jin, Y.; He, S. Ultra-broadband microwave metamaterial absorber. *Appl. Phys. Lett.* **2012**, *100*, 103506. [CrossRef]
22. Wu, Z.; Zhang, Z.L.; Chen, X.Q.; Feng, F.; Zhang, L.; Lv, Y.Y.; He, Y.Y.; Zou, Y.H. Microwave scattering-absorption properties of a lightweight all-dielectric coding metamaterial based on TiO_2/CNTs. *Opt. Lett.* **2020**, *45*, 555–558. [CrossRef]
23. Datta, S.; Mukherjee, S.; Shi, X.D.; Haq, M.; Deng, Y.M.; Udpa, L.; Rothwell, E. Negative index metamaterial lens for subwavelength microwave detection. *Sensors* **2021**, *21*, 4782. [CrossRef]
24. Xu, J.; Fan, Y.C.; Su, X.P.; Guo, J.; Zhu, J.X.; Fu, Q.H.; Zhang, F.L. Broadband and wide angle microwave absorption with optically transparent metamaterial. *Opt. Mater.* **2021**, *113*, 110852. [CrossRef]
25. Wang, Y.; Sun, T.; Paudel, T.; Zhang, Y.; Ren, Z.; Kempa, K. Metamaterial-plasmonic absorber structure for high efficiency amorphous silicon solar cells. *Nano Lett.* **2012**, *12*, 440–445. [CrossRef]
26. Watts, C.M.; Liu, X.; Padilla, W.J. Metamaterial electromagnetic wave absorbers. *Adv. Mater.* **2012**, *24*, OP98–OP120. [CrossRef] [PubMed]
27. Cong, L.; Cao, W.; Zhang, X.; Tian, Z.; Gu, J.; Singh, R.; Han, J.; Zhang, W. A perfect metamaterial polarization rotator. *Appl. Phys. Lett.* **2013**, *103*, 171107. [CrossRef]
28. Withayachumnankul, W.; Jaruwongrungsee, K.; Tuantranont, A.; Fumeaux, C.; Abbott, D. Metamaterial-based microfluidic sensor for dielectric characterization. *Sens. Actuators A Phys.* **2013**, *189*, 233–237. [CrossRef]
29. Yu-Sheng, L.; Chia-Yi, H.; Chengkuo, L. Reconfiguration of resonance characteristics for terahertz U-shape metamaterial using MEMS mechanism. *IEEE J. Sel. Top. Quantum Electron.* **2015**, *21*, 93–99. [CrossRef]
30. Lochbaum, A.; Fedoryshyn, Y.; Dorodnyy, A.; Koch, U.; Hafner, C.; Leuthold, J. On-chip narrowband thermal emitter for Mid-IR optical gas sensing. *ACS Photonics* **2017**, *4*, 1371–1380. [CrossRef]
31. Appavoo, K.; Haglund, R.F. Detecting nanoscale size dependence in VO_2 phase transition using a split-ring resonator metamaterial. *Nano Lett.* **2011**, *11*, 1025–1031. [CrossRef]
32. Wang, H.; Yang, Y.; Wang, L. Switchable wavelength-selective and diffuse metamaterial absorber/emitter with a phase transition spacer layer. *Appl. Phys. Lett.* **2014**, *105*, 071907. [CrossRef]
33. Lei, L.; Lou, F.; Tao, K.Y.; Huang, H.X.; Cheng, X.; Xu, P. Tunable and scalable broadband metamaterial absorber involving VO2-based phase transition. *Photonics Res.* **2019**, *7*, 734–741. [CrossRef]
34. Chen, P.-Y.; Alu, A. Terahertz metamaterial devices based on graphene nanostructures. *IEEE Trans. Terahertz Sci. Technol.* **2013**, *3*, 748–756. [CrossRef]
35. Zhang, Y.; Li, T.; Chen, Q.; Zhang, H.; O'Hara, J.F.; Abele, E.; Taylor, A.J.; Chen, H.T.; Azad, A.K. Independently tunable dual-band perfect absorber based on graphene at mid-infrared frequencies. *Sci. Rep.* **2015**, *5*, 18463. [CrossRef]
36. Li, H.; Wang, L.; Zhai, X. Tunable graphene-based mid-infrared plasmonic wide-angle narrowband perfect absorber. *Sci. Rep.* **2016**, *6*, 36651. [CrossRef] [PubMed]
37. Zhang, J.; Wang, G.; Zhang, B.; He, T.; He, Y.; Shen, J. Photo-excited broadband tunable terahertz metamaterial absorber. *Opt. Mater.* **2016**, *54*, 32–36. [CrossRef]
38. Shrekenhamer, D.; Chen, W.C.; Padilla, W.J. Liquid crystal tunable metamaterial absorber. *Phys. Rev. Lett.* **2013**, *110*, 177403. [CrossRef] [PubMed]
39. Ou, J.Y.; Plum, E.; Zhang, J.; Zheludev, N.I. Giant nonlinearity of an optically reconfigurable plasmonic metamaterial. *Adv. Mater.* **2016**, *28*, 729–733. [CrossRef] [PubMed]
40. Kim, J.; Jeong, H.; Lim, S. Mechanically actuated frequency reconfigurable metamaterial absorber. *Sens. Actuators A Phys.* **2019**, *299*, 111619. [CrossRef]
41. Zhu, W.M.; Liu, A.Q.; Zhang, W.; Tao, J.F.; Bourouina, T.; Teng, J.H.; Zhang, X.H.; Wu, Q.Y.; Tanoto, H.; Guo, H.C.; et al. Polarization dependent state to polarization independent state change in THz metamaterials. *Appl. Phys. Lett.* **2011**, *99*. [CrossRef]
42. Zhu, W.M.; Liu, A.Q.; Bourouina, T.; Tsai, D.P.; Teng, J.H.; Zhang, X.H.; Lo, G.Q.; Kwong, D.L.; Zheludev, N.I. Microelectromechanical Maltese-cross metamaterial with tunable terahertz anisotropy. *Nat. Commun.* **2012**, *3*, 1274. [CrossRef]
43. Liu, X.; Padilla, W.J. Dynamic manipulation of infrared radiation with MEMS metamaterials. *Adv. Opt. Mater.* **2013**, *1*, 559–562. [CrossRef]
44. Ho, C.P.; Pitchappa, P.; Lin, Y.-S.; Huang, C.-Y.; Kropelnicki, P.; Lee, C. Electrothermally actuated microelectromechanical systems based omega-ring terahertz metamaterial with polarization dependent characteristics. *Appl. Phys. Lett.* **2014**, *104*, 161104. [CrossRef]
45. Pitchappa, P.; Ho, C.P.; Dhakar, L.; Lee, C. Microelectromechanically reconfigurable interpixelated metamaterial for independent tuning of multiple resonances at terahertz spectral region. *Optica* **2015**, *2*, 571–578. [CrossRef]
46. Pitchappa, P.; Ho, C.P.; Cong, L.; Singh, R.; Singh, N.; Lee, C. Reconfigurable digital metamaterial for dynamic switching of terahertz anisotropy. *Adv. Opt. Mater.* **2016**, *4*, 391–398. [CrossRef]
47. Liu, X.; Padilla, W.J. Reconfigurable room temperature metamaterial infrared emitter. *Optica* **2017**, *4*, 430–433. [CrossRef]
48. Zhao, X.; Schalch, J.; Zhang, J.; Seren, H.R.; Duan, G.; Averitt, R.D.; Zhang, X. Electromechanically tunable metasurface transmission waveplate at terahertz frequencies. *Optica* **2018**, *5*, 303–310. [CrossRef]
49. Xu, Z.; Lin, Y.S. A stretchable terahertz parabolic-shaped metamaterial. *Adv. Opt. Mater.* **2019**, *7*, 1900379. [CrossRef]
50. Mo, Y.; Zhong, J.; Lin, Y.-S. Tunable chevron-shaped infrared metamaterial. *Mater. Lett.* **2020**, *263*, 127291. [CrossRef]

51. Xu, R.; Lin, Y.S. Flexible and controllable metadevice using self-assembly MEMS actuator. *Nano Lett.* **2021**, *21*, 3205–3210. [CrossRef]
52. Ou, J.Y.; Plum, E.; Jiang, L.; Zheludev, N.I. Reconfigurable photonic metamaterials. *Nano Lett.* **2011**, *11*, 2142–2144. [CrossRef]
53. Pitchappa, P.; Ho, C.P.; Kropelnicki, P.; Singh, N.; Kwong, D.L.; Lee, C. Micro-electro-mechanically switchable near infrared complementary metamaterial absorber. *Appl. Phys. Lett.* **2014**, *104*, 201114. [CrossRef]
54. Ivzhenko, L.; Odarenko, E.; Tarapov, S.I. Mechanically tunable wire medium metamaterial in the millimeter wave band. *Prog. Electromagn. Res.* **2016**, *64*, 93–98. [CrossRef]
55. Liu, J.J.; Hong, Z. Mechanically tunable dual frequency THz metamaterial filter. *Opt. Commun.* **2018**, *426*, 598–601. [CrossRef]
56. Morris, C.; Bekker, L.; Spadaccini, C.; Haberman, M.; Seepersad, C. Tunable mechanical metamaterial with constrained negative stiffness for improved quasi-static and dynamic energy dissipation. *Adv. Eng. Mater.* **2019**, *21*, 1900163. [CrossRef]
57. Chen, F.Q.; Liu, X.J.; Tian, Y.P.; Zheng, Y. Mechanically stretchable metamaterial with tunable mid-infrared optical properties. *Opt. Express* **2021**, *29*, 37368–37375. [CrossRef] [PubMed]
58. Tao, H.; Strikwerda, A.C.; Fan, K.; Padilla, W.J.; Zhang, X.; Averitt, R.D. Reconfigurable terahertz metamaterials. *Phys. Rev. Lett.* **2009**, *103*, 147401. [CrossRef] [PubMed]
59. Pitchappa, P.; Manjappa, M.; Krishnamoorthy, H.N.S.; Chang, Y.; Lee, C.; Singh, R. Bidirectional reconfiguration and thermal tuning of microcantilever metamaterial device operating from 77 K to 400 K. *Appl. Phys. Lett.* **2017**, *111*, 261101. [CrossRef]
60. Zhong, J.; Xu, X.; Lin, Y.-S. Tunable terahertz metamaterial with electromagnetically induced transparency characteristic for sensing application. *Nanomaterials* **2021**, *11*, 2175. [CrossRef]
61. Yang, J.; Lin, Y.-S. Design of tunable terahertz metamaterial sensor with single- and dual-resonance characteristic. *Nanomaterials* **2021**, *11*, 2212. [CrossRef] [PubMed]
62. Xu, R.; Xu, X.; Yang, B.-R.; Gui, X.; Qin, Z.; Lin, Y.-S. Actively logical modulation of MEMS-based terahertz metamaterial. *Photonics Res.* **2021**, *9*. [CrossRef]
63. Li, X.; Yang, T.; Zhu, W.; Li, X. Continuously tunable terahertz metamaterial employing a thermal actuator. *Microsyst. Technol.* **2012**, *19*, 1145–1151. [CrossRef]
64. Lalas, A.; Kantartzis, N.; Tsiboukis, T. Programmable terahertz metamaterials through V-beam electrothermal devices. *Appl. Phys. A* **2014**, *117*, 433–438. [CrossRef]
65. Lalas, A.X.; Kantartzis, N.V.; Tsiboukis, T.D. Reconfigurable metamaterial components exploiting two-hot-arm electrothermal actuators. *Microsyst. Technol.* **2015**, *21*, 2097–2107. [CrossRef]
66. Lin, Y.-S.; Qian, Y.; Ma, F.; Liu, Z.; Kropelnicki, P.; Lee, C. Development of stress-induced curved actuators for a tunable THz filter based on double split-ring resonators. *Appl. Phys. Lett.* **2013**, *102*, 111908. [CrossRef]
67. Liu, M.; Susli, M.; Silva, D.; Putrino, G.; Kala, H.; Fan, S.; Cole, M.; Faraone, L.; Wallace, V.P.; Padilla, W.J.; et al. Ultrathin tunable terahertz absorber based on MEMS-driven metamaterial. *Microsyst. Nanoeng.* **2017**, *3*, 17033. [CrossRef]
68. Manjappa, M.; Pitchappa, P.; Singh, N.; Wang, N.; Zheludev, N.I.; Lee, C.; Singh, R. Reconfigurable MEMS Fano metasurfaces with multiple-input-output states for logic operations at terahertz frequencies. *Nat. Commun.* **2018**, *9*, 4056. [CrossRef] [PubMed]
69. Lin, Y.S.; Ma, F.; Lee, C. Three-dimensional movable metamaterial using electric split-ring resonators. *Opt. Lett.* **2013**, *38*, 3126–3128. [CrossRef]
70. Pitchappa, P.; Ho, C.P.; Dhakar, L.; Qian, Y.; Singh, N.; Lee, C. Periodic array of subwavelength MEMS cantilevers for dynamic manipulation of terahertz waves. *J. Microelectromech. Syst.* **2015**, *24*, 525–527. [CrossRef]
71. Zhengli, H.; Kohno, K.; Fujita, H.; Hirakawa, K.; Toshiyoshi, H. Tunable terahertz filter and modulator based on electrostatic MEMS reconfigurable SRR array. *IEEE J. Sel. Top. Quantum Electron.* **2015**, *21*, 114–122. [CrossRef]
72. Shih, K.; Pitchappa, P.; Manjappa, M.; Ho, C.P.; Singh, R.; Yang, B.; Singh, N.; Lee, C. Active MEMS metamaterials for THz bandwidth control. *Appl. Phys. Lett.* **2017**, *110*, 161108. [CrossRef]
73. Pitchappa, P.; Ho, C.P.; Qian, Y.; Dhakar, L.; Singh, N.; Lee, C. Microelectromechanically tunable multiband metamaterial with preserved isotropy. *Sci. Rep.* **2015**, *5*, 11678. [CrossRef] [PubMed]
74. Pitchappa, P.; Manjappa, M.; Ho, C.P.; Qian, Y.; Singh, R.; Singh, N.; Lee, C. Active control of near-field coupling in conductively coupled microelectromechanical system metamaterial devices. *Appl. Phys. Lett.* **2016**, *108*, 111102. [CrossRef]
75. Ma, F.; Qian, Y.; Lin, Y.-S.; Liu, H.; Zhang, X.; Liu, Z.; Ming-Lin Tsai, J.; Lee, C. Polarization-sensitive microelectromechanical systems based tunable terahertz metamaterials using three dimensional electric split-ring resonator arrays. *Appl. Phys. Lett.* **2013**, *102*, 161912. [CrossRef]
76. Lin, Y.-S.; Lee, C. Tuning characteristics of mirrorlike T-shape terahertz metamaterial using out-of-plane actuated cantilevers. *Appl. Phys. Lett.* **2014**, *104*, 251914. [CrossRef]
77. Schalch, J.; Duan, G.W.; Zhao, X.G.; Zhang, X.; Averitt, R.D. Terahertz metamaterial perfect absorber with continuously tunable air spacer layer. *Appl. Phys. Lett.* **2018**, *113*, 061113. [CrossRef]
78. Liu, S.; Zhang, L.; Bai, G.D.; Cui, T.J. Flexible controls of broadband electromagnetic wavefronts with a mechanically programmable metamaterial. *Sci. Rep.* **2019**, *9*, 1809. [CrossRef]
79. Wang, J.; Tian, H.; Wang, G.C.; Li, S.; Guo, W.P.; Xing, J.; Wang, Y.; Li, L.; Zhou, Z.X. Mechanical control of terahertz plasmon-induced transparency in single/double-layer stretchable metamaterial. *J. Phys. D Appl. Phys.* **2021**, *54*, 035101. [CrossRef]

80. Fu, Y.H.; Liu, A.Q.; Zhu, W.M.; Zhang, X.M.; Tsai, D.P.; Zhang, J.B.; Mei, T.; Tao, J.F.; Guo, H.C.; Zhang, X.H.; et al. A micromachined reconfigurable metamaterial via reconfiguration of asymmetric split-ring resonators. *Adv. Funct. Mater.* **2011**, *21*, 3589–3594. [CrossRef]
81. Zhu, W.M.; Liu, A.Q.; Zhang, X.M.; Tsai, D.P.; Bourouina, T.; Teng, J.H.; Zhang, X.H.; Guo, H.C.; Tanoto, H.; Mei, T.; et al. Switchable magnetic metamaterials using micromachining processes. *Adv. Mater.* **2011**, *23*, 1792–1796. [CrossRef] [PubMed]
82. Wu, Z.; Wei Ming, Z.; Hong, C.; Tsai, M.L.J.; Guo-Qiang, L.; Din Ping, T.; Tanoto, H.; Jing-Hua, T.; Xin-Hai, Z.; Dim-Lee, K.; et al. Resonance switchable metamaterials using MEMS fabrications. *IEEE J. Sel. Top. Quantum Electron.* **2013**, *19*, 4700306. [CrossRef]
83. Zhao, X.; Fan, K.; Zhang, J.; Keiser, G.R.; Duan, G.; Averitt, R.D.; Zhang, X. Voltage-tunable dual-layer terahertz metamaterials. *Microsyst. Nanoeng.* **2016**, *2*, 16025. [CrossRef]
84. Huang, Y.; Nakamura, K.; Takida, Y.; Minamide, H.; Hane, K.; Kanamori, Y. Actively tunable THz filter based on an electromagnetically induced transparency analog hybridized with a MEMS metamaterial. *Sci. Rep.* **2020**, *10*, 20807. [CrossRef] [PubMed]
85. Zhang, M.; Zhang, W.; Liu, A.Q.; Li, F.C.; Lan, C.F. Tunable polarization conversion and rotation based on a reconfigurable metasurface. *Sci. Rep.* **2017**, *7*, 12068. [CrossRef] [PubMed]
86. Wen, Y.; Liang, Z.; Lin, Y.-S.; Chen, C.-H. Active modulation of polarization-sensitive infrared metamaterial. *Opt. Commun.* **2020**, *463*, 125489. [CrossRef]
87. Xu, T.; Lin, Y.-S. Tunable terahertz metamaterial using an electric split-ring resonator with polarization-sensitive characteristic. *Appl. Sci.* **2020**, *10*, 4660. [CrossRef]
88. Xu, T.; Xu, R.; Lin, Y.-S. Tunable terahertz metamaterial using electrostatically electric split-ring resonator. *Results Phys.* **2020**, *19*, 103638. [CrossRef]
89. Xu, T.; Xu, X.; Lin, Y.-S. Tunable terahertz free spectra range using electric split-ring metamaterial. *J. Microelectromech. Syst.* **2021**, *30*, 309–314. [CrossRef]
90. Zheludev, N.I.; Plum, E. Reconfigurable nanomechanical photonic metamaterials. *Nat. Nanotechnol.* **2016**, *11*, 16–22. [CrossRef]
91. Kang, L.; Zhao, Q.; Zhao, H.J.; Zhou, J. Ferrite-based magnetically tunable left-handed metamaterial composed of SRRs and wires. *Opt. Express* **2008**, *16*, 17269–17275. [CrossRef] [PubMed]
92. Cho, I.-J.; Yoon, E. A low-voltage three-axis electromagnetically actuated micromirror for fine alignment among optical devices. *J. Micromech. Microeng.* **2009**, *19*, 085007. [CrossRef]
93. Ozbey, B.; Aktas, O. Continuously tunable terahertz metamaterial employing magnetically actuated cantilevers. *Opt. Express* **2011**, *19*, 5741–5752. [CrossRef] [PubMed]
94. Khodasevych, I.E.; Shah, C.M.; Rowe, W.S.T.; Mitchell, A. Flexible fishnet metamaterial on PDMS substrate for THz frequencies. In Proceedings of the 2010 Conference on Optoelectronic and Microelectronic Materials and Devices, Canberra, Australia, 12–15 December 2010; pp. 25–26.
95. Ling, K.; Kim, K.; Lim, S. Flexible liquid metal-filled metamaterial absorber on polydimethylsiloxane (PDMS). *Opt. Express* **2015**, *23*, 21375–21383. [CrossRef]
96. Malek, S.C.; Ee, H.S.; Agarwal, R. Strain multiplexed metasurface holograms on a stretchable substrate. *Nano Lett.* **2017**, *17*, 3641–3645. [CrossRef]
97. Li, J.; Shah, C.M.; Withayachumnankul, W.; Ung, B.S.Y.; Mitchell, A.; Sriram, S.; Bhaskaran, M.; Chang, S.; Abbott, D. Mechanically tunable terahertz metamaterials. *Appl. Phys. Lett.* **2013**, *102*, 012110. [CrossRef]
98. Zhang, F.; Feng, S.; Qiu, K.; Liu, Z.; Fan, Y.; Zhang, W.; Zhao, Q.; Zhou, J. Mechanically stretchable and tunable metamaterial absorber. *Appl. Phys. Lett.* **2015**, *106*, 091907. [CrossRef]
99. Kim, K.; Lee, D.; Eom, S.; Lim, S. Stretchable metamaterial absorber using liquid metal-filled polydimethylsiloxane (PDMS). *Sensors* **2016**, *16*, 521. [CrossRef]
100. Ee, H.S.; Agarwal, R. Tunable metasurface and flat optical zoom lens on a stretchable substrate. *Nano Lett.* **2016**, *16*, 2818–2823. [CrossRef]
101. Xu, R.; Luo, J.; Sha, J.; Zhong, J.; Xu, Z.; Tong, Y.; Lin, Y.-S. Stretchable IR metamaterial with ultra-narrowband perfect absorption. *Appl. Phys. Lett.* **2018**, *113*, 101907. [CrossRef]
102. Zhang, H.; Feng, L.; Liang, Y.Z.; Xu, T. An ultra-flexible plasmonic metamaterial film for efficient omnidirectional and broadband optical absorption. *Nanoscale* **2019**, *11*, 437–443. [CrossRef]
103. Gao, Z.Q.; Xu, C.L.; Tian, X.X.; Wang, J.F.; Tian, C.H.; Yang, B.Y.; Qu, S.B.; Fan, Q. Ultra-wideband flexible transparent metamaterial with wide-angle microwave absorption and low infrared emissivity. *Opt. Express* **2021**, *29*, 22108–22116. [CrossRef]
104. Ahamed, E.; Faruque, M.R.I.; Alam, M.J.; Bin Mansor, M.F.; Islam, M.T. Digital metamaterial filter for encoding information. *Sci. Rep.* **2020**, *10*, 3289. [CrossRef]
105. Cong, L.; Pitchappa, P.; Lee, C.; Singh, R. Active phase transition via loss engineering in a terahertz MEMS metamaterial. *Adv. Mater.* **2017**, *29*, 1700733. [CrossRef]
106. Manjappa, M.; Pitchappa, P.; Wang, N.; Lee, C.; Singh, R. Active control of resonant cloaking in a terahertz MEMS metamaterial. *Adv. Opt. Mater.* **2018**, *6*, 1800141. [CrossRef]
107. Xu, Z.; Lin, Z.; Cheng, S.; Lin, Y.S. Reconfigurable and tunable terahertz wrench-shape metamaterial performing programmable characteristic. *Opt. Lett.* **2019**, *44*, 3944–3947. [CrossRef] [PubMed]

108. Zhu, F.; Lin, Y.-S. Programmable multidigit metamaterial using terahertz electric spilt-ring resonator. *Opt. Laser Technol.* **2021**, *134*, 106635. [CrossRef]
109. Ho, C.P.; Pitchappa, P.; Lee, C. Digitally reconfigurable binary coded terahertz metamaterial with output analogous to NOR and AND. *J. Appl. Phys.* **2016**, *119*, 153104. [CrossRef]
110. Lin, P.-S.; Shen, T.-W.; Chan, K.-C.; Fang, W. CMOS MEMS thermoelectric infrared sensor with plasmonic metamaterial absorber for selective wavelength absorption and responsivity enhancement. *IEEE Sens. J.* **2020**, *20*, 11105–11114. [CrossRef]
111. Hui, Y.; Gomez-Diaz, J.S.; Qian, Z.; Alu, A.; Rinaldi, M. Plasmonic piezoelectric nanomechanical resonator for spectrally selective infrared sensing. *Nat. Commun.* **2016**, *7*, 11249. [CrossRef]
112. Zhang, Y.; Lin, P.; Lin, Y.S. Tunable split-disk metamaterial absorber for sensing application. *Nanomaterials* **2021**, *11*, 598. [CrossRef]
113. Zhao, X.; Yang, B.; Liu, J.; Pitchappa, P.; Hasan, D.; Ho, C.P.; Yang, C.; Lee, C. A multiband flexible terahertz metamaterial with curvature sensing functionality. *J. Opt.* **2016**, *18*, 075101. [CrossRef]
114. Wen, Y.; Liang, Z.; Lin, Y.-S. Tunable perfect meta-absorber with high-sensitive polarization characteristic. *Adv. Photonics Res.* **2020**, *2*, 2000027. [CrossRef]
115. Annamdas, V.G.M.; Soh, C.K. A perspective of non-fiber-optical metamaterial and piezoelectric material sensing in automated structural health monitoring. *Sensors* **2019**, *19*, 1490. [CrossRef] [PubMed]
116. Wang, W.; Yan, F.P.; Tan, S.Y.; Li, H.S.; Du, X.M.; Zhang, L.N.; Bai, Z.Y.; Cheng, D.; Zhou, H.; Hou, Y.F. Enhancing sensing capacity of terahertz metamaterial absorbers with a surface-relief design. *Photonics Res.* **2020**, *8*, 519–527. [CrossRef]
117. Du, X.M.; Yan, F.P.; Wang, W.; Zhang, L.N.; Bai, Z.Y.; Zhou, H.; Hou, Y.F. Thermally-stable graphene metamaterial absorber with excellent tunability for high-performance refractive index sensing in the terahertz band. *Opt. Laser Technol.* **2021**, *144*, 107409. [CrossRef]
118. Gao, H.X.; Liang, Y.Z.; Yu, L.; Chu, S.W.; Cai, L.N.; Wang, F.; Wang, Q.; Peng, W. Bifunctional plasmonic metamaterial absorber for narrowband sensing detection and broadband optical absorption. *Opt. Laser Technol.* **2021**, *137*, 106807. [CrossRef]
119. Liu, W.X.; Ma, Y.M.; Chang, Y.H.; Dong, B.W.; Wei, J.X.; Ren, Z.H.; Lee, C.K. Suspended silicon waveguide platform with subwavelength grating metamaterial cladding for long-wave infrared sensing applications. *Nanophotonics* **2021**, *10*, 1861–1870. [CrossRef]
120. Yu, J.; Lang, T.T.; Chen, H.T. All-metal terahertz metamaterial absorber and refractive index sensing performance. *Photonics* **2021**, *8*, 164. [CrossRef]